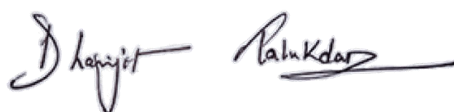


*Dedicated to my
parents & my brother*

Declaration by the Candidate

I, **Dhanjit Talukdar**, declare that the thesis entitled “**Investigation of electronic, optical, and surface adsorption properties in engineered black phosphorene and its isostructural tin sulfide systems**” is a record of my own work carried out under the supervision of **Prof. Gazi Ameen Ahmed** during the period from October, 2021 to May, 2025. I confirm that:

- This work was done wholly or mainly while in candidature for a research degree in Doctor of Philosophy at Tezpur University where no part of this thesis has previously been submitted for a degree or any other qualification at this university or any other institution.
- Where I have quoted from the work of others, the source is always given. With the exception of such quotations, this thesis is entirely my own work. I have acknowledged all main sources of help.
- Where the thesis is based on work done by myself jointly with others, I have made clear exactly what was done by others and what I have contributed myself.



(Dhanjit Talukdar)

Date: 8th September, 2025

Place: Tezpur, Assam, India

Registration No. TZ24003131 of 2024



Tezpur University

(A Central University established by an Act of Parliament)

Tezpur- 784028 :: Assam

Gazi Ameen Ahmed

Professor

Department of Physics

Tezpur University

Email: gazi@tezu.ernet.in

Phone: 03712-275556 (O)

Mobile: 9435014377

Certificate by the Supervisor

This is to certify that the thesis entitled “**Investigation of electronic, optical, and surface adsorption properties in engineered black phosphorene and its isostructural tin sulfide systems**”, submitted to the School of Sciences, Tezpur University in partial fulfilment for the award of the degree of **Doctor of Philosophy** in Physics is a record of original research work carried out by **Mr. Dhanjit Talukdar** under my supervision and guidance.

All help received by him from various sources have been duly acknowledged. No part of this thesis has been submitted elsewhere for award of any other degree.

Date: 8th September, 2025

Place: Tezpur, Assam, India

Prof. Gazi Ameen Ahmed
Professor, Department of Physics
Tezpur University

Acknowledgements

I would like to express my heartfelt gratitude and deep appreciation to all those whose support and encouragement made my Ph.D. journey possible. First and foremost, I am profoundly thankful to my supervisor, Prof. Gazi Ameen Ahmed, for believing in me and giving me the opportunity to pursue my doctoral studies under his guidance. His trust and support have been instrumental in shaping my academic journey. I am especially grateful for the intellectual freedom he provided, which allowed me to explore, learn, and develop essential skills in the field.

I extend my sincere gratitude to my doctoral committee members, Prof. Pritam Deb and Prof. Dambarudhar Mohanta, for their valuable suggestions and insightful discussions, which greatly enriched my research. I am especially thankful to Prof. Mohanta for graciously allowing me to participate in his group meetings, which played a significant role in framing the direction of my research work. I also wish to express my appreciation to the former and present Heads of the Department, as well as all the faculty members, for their constant encouragement and support throughout my doctoral journey. I am grateful to Tezpur University for providing the fellowship that supported me during this time. I am also thankful to Prof. Nidhi S. Bhattacharyya for her consistent encouragement to take part in extracurricular activities, which contributed meaningfully to my personal growth. I extend my gratitude to the office staff of the department, especially Narayan da and Suman da, for their kind assistance and constant support in handling various administrative matters with patience and efficiency.

For a Ph.D. scholar in theoretical physics, computing facilities are the lifeline of research. I gratefully acknowledge the computational support that made my research work possible. I sincerely thank Tezpur University for providing access to the PARAM Tez high-performance computing system, as well as the Department of Physics, Tezpur University, for access to its dedicated HPC resources. I also acknowledge the support of the National Supercomputing Mission (NSM) for providing access to the 'PARAM Porul' supercomputing facility at NIT Trichy, implemented by C-DAC and supported by MeitY and DST, Government of India.

It gives me immense pleasure to thank my collaborators, Prof. Dambarudhar Mohanta and Ms. Bhupali Deka from the Department of Physics, Tezpur University, as well

as Prof. Devasish Chowdhury and Mr. Bitopan Boro from IASST, Guwahati, for their valuable contributions and support.

I would like to extend my heartfelt thanks to all the former and present research scholars in the department. While it is difficult to name everyone, I would like to thank Olag da, Hirak da, Sunny da, Sritam da, Hemanga da, Ritu da, Abinash da, Saransha da, Amrita ba, and Tanushree. A special word of thanks goes to Prankrishna da for bringing a joyful and creative dimension to my university life through our involvement in short films. I am truly fortunate to have some wonderful friends, especially Anil, Niranjana, Jubaraj, Debasish, and Hritwik. A special mention goes to Anil for always being there to help me with DFT discussions. I would also like to thank my former and present labmates Kabita ba, Nishant da, Kaushik, Janmejyoti, Shahnaz, Debasish, Himakshi, Udipta, and Rahul. I am also grateful to the members of the NSL lab, Aftab da, Kakoli ba, Ankush da, Stuti, Susmita, Bikash, Anuj, Dipankar, Saddique, and Satyajit, for welcoming me as a member of their group. I am also deeply grateful to my friend-cum-mentors, Goutam, Bitopan, Jintu, Hirak, and Joseph, for their constant motivation, guidance, and belief in me, which have made a lasting impact on both my academic and personal journey.

My deepest gratitude goes to Bhupali, my constant support, my companion through both happiness and sorrow. Her unwavering presence, patience, and encouragement have been a source of strength throughout this journey, and I am truly fortunate to have her by my side.

Finally, I am truly indebted to my Maa, Papa, and Moni. It is because of their constant support that I am standing where I am today. Their immense love, sacrifices, and enduring strength have shaped me, given me the courage to persevere through every challenge, and continue to inspire me to pursue my dreams.

Above all, I thank the Almighty for giving me the strength, clarity, and patience to navigate this journey and for guiding me every step of the way.

Dhanjit Talukdar

List of Tables

Table No.	Table title	Page. No.
Table 1.1	Vacancy formation energies of BP, graphene, silicene, WSe ₂ , and SnS.	5
Table 3.1	Lattice parameters of the 3×3 BP _V ^N supercell under different uniaxial strain along the zz and ac direction.	44
Table 3.2	Band gaps and magnetic moments of BP _V ^N monolayer under tensile and compressive strain along zz direction.	46
Table 3.3	Band gaps and magnetic moments of BP _V ^N monolayer under tensile and compressive strain along ac direction.	48
Table 4.1	Adsorption energy (E_{ad}), charge transferred (ΔQ) between the layer and the molecule, minimum distance (d) between the atoms of the layer and the molecule (closest atoms are mentioned within the brackets), and the nature of adsorption of NO ₂ , SO ₂ , CO, CO ₂ , and NH ₃ , molecules.	57
Table 5.1	Lattice parameters of the monolayer supercells and the strain experienced by them within the heterostructure.	76
Table 5.2	Indirect and direct band gaps of SnS/ <i>h</i> -BN heterostructure and SnS monolayer along with their direction in the BZ calculated at the GW and DFT-GGA level. The last column shows the difference between the band gaps of SnS monolayer and SnS/ <i>h</i> -BN heterostructure.	79
Table 5.3	Calculated charge carrier effective mass of SnS/ <i>h</i> -BN heterostructure and SnS monolayer.	82
Table 5.4	The excitonic peak positions and exciton binding energy (EBE) of SnS/ <i>h</i> -BN heterostructure (Fig. 5.6(a)) and SnS monolayer (Fig. 5.6(b)) along with their respective direct band gap position in the BZ momentum space. The last two	83

rows show the results of SnS monolayer under the compressive strain of 1.23% and 0.67% along the x - and y -direction, respectively.

Table 6.1	Structural parameters, electronic band gap (E_g^{GGA} and E_g^{GW}), exciton peaks, and exciton binding energies (EBE) of SnS monolayer and zigzag BNNTs.	95
Table 6.2	Direct and indirect electronic band gaps of the heterostructures along with their direction/position in the momentum space at DFT-GGA (E_g^{GGA}) and GW (E_g^{GW}) level of calculation.	100
Table 6.3	Excitonic peak positions and EBEs for the A_{SnS} (Γ -Y) and B_{SnS} (Γ -X) excitons, along with the corresponding direct band gaps of the three SnS/BNNT heterostructures. For reference, the values for the pristine SnS monolayer are also included.	103
Table 6.4	Peak positions of the IDEs under tensile strain.	107
Table A.3	Initial positions of molecules before atomic relaxation on BP_v^{N} monolayer and their respective adsorption energy after atomic relaxation.	119

List of Figures

Figure No.	Figure caption	Page. No.
Figure 1.1	Different allotropes of carbon-based quantum confined material.	1
Figure 1.2	Optimized geometrical structures of (a-c) BP and (d-f) SnS monolayers (3×3 supercell). Panels (a) and (d), and (b) and (e) show side views along the armchair and zigzag directions, respectively, while panels (c) and (f) present the top views.	3
Figure 1.3	Schematic overview of the research works presented in the thesis. Chapters 3 and 4 focus on defect engineering in BP, while Chapters 5 and 6 explore heterostructure engineering involving SnS-based systems.	9
Figure 2.1	Comparison between the wavefunction in the true Coulomb potential of the nucleus (blue) and that in the corresponding pseudopotential (red). Both the wavefunctions and the potentials coincide beyond a specific cutoff radius r_c . (Image source: https://en.wikipedia.org/wiki/Pseudopotential).	26
Figure 3.1	(a) Top view, and (b) side view of 3×3 supercell of pristine BP; (c) BP with a P vacancy (BP_v), and (d) BP with a doped N atom (BP^N).	38
Figure 3.2	(a-d) Four different configurations of compound defect in BP; (e) side view (along ac direction) of the four possible configurations of the compound defect in BP; (f) ground state energy of the four configurations.	38
Figure 3.3	Schematic depicting the formation of compound defect in BP.	40
Figure 3.4	AIMD simulation of BP_v^N at (a) 300 K and (b) 600 K over a time period of 8.5 ps (the axis on the left side of the figures	41

represents the energy of the heterostructure and the axis on the right side of the figures represents the temperature scale).

Figure 3.5	Electronic band structure (spin up and spin down bands are indicated by pink and blue colours, respectively) and DOS plots of (a) pristine BP, (b) BP^N , (c) BP_v , and (d) BP_v^N system.	43
Figure 3.6	PDOS of (a) pristine BP, (b) BP^N , (c) BP_v , and (d) BP_v^N system.	44
Figure 3.7	Band structure of BP_v^N monolayer under (a) 1% strain, (b) 3% strain, (c) 5% strain along the zz direction, respectively; (d) band gap values of BP_v^N under tensile along the zz direction; (spin up and spin down bands are indicated by pink and blue colours, respectively).	45
Figure 3.8	Band structure of BP_v^N monolayer under (a) -1% strain, (b) -3% strain, (c) -5% strain along the zz direction, respectively; (d) band gap values of BP_v^N under compressive along the zz direction; (spin up and spin down bands are indicated by pink and blue colours, respectively).	46
Figure 3.9	Band structure of BP_v^N monolayer under (a) 1% strain, (b) 3% strain, (c) 5% strain along the ac direction, respectively; (d) band gap values of BP_v^N under tensile along the ac direction; (spin up and spin down bands are indicated by pink and blue colours, respectively).	47
Figure 3.10	Band structure of BP_v^N monolayer under (a) -1% strain, (b) -3% strain, (c) -5% strain along the ac direction, respectively; (d) band gap values of BP_v^N under compressive along the ac direction; (spin up and spin down bands are indicated by pink and blue colours, respectively).	48

Figure 4.1	Relaxed structures of (a) BP_V^N , (b) BP_V , and (c) BP^N sheet; (d) top view and (e, f) side view of charge density difference in BP_V^N sheet (note that the region in green and purple represents accumulated and depleted charged regions, respectively).	54
Figure 4.2	Relaxed structures of adsorbed (a-c) NO_2 and (e-g) SO_2 on BP_V^N , BP_V , and BP^N surface, respectively. Charge density difference of BP_V^N after adsorption of (d) NO_2 , and (h) SO_2 molecules (purple regions represent the depletion and green regions represents an accumulation of charges).	58
Figure 4.3	Electron localisation function (ELF) plots of (a-c) NO_2 , and (d-f) SO_2 on BP_V^N , BP_V , and BP^N surfaces, respectively.	58
Figure 4.4	DOS (upper stack) and projected DOS (lower stack) of BP_V^N , BP_V , and BP^N sheet before and after adsorption of (a-c) NO_2 , and (d-f) SO_2 molecules, respectively (red and black colour indicates DOS before and after adsorption; dark yellow and purple colour indicates s orbital, pink and violet colour indicates p orbital of N and O atom, respectively).	59
Figure 4.5	Relaxed structures and DOS of BP_V^N sheet after (a,d) CO, (b,e) CO_2 , and (c,f) NH_3 adsorption, respectively (red and black colour indicates DOS before and after adsorption; dark yellow and purple colour indicates s orbital, pink and violet colour indicates p orbital of N and O atom, respectively).	62
Figure 4.6	Relaxed structures of BP_V , and BP^N sheet after (a,d) CO, (b,e) CO_2 , and (c,f) NH_3 adsorption, respectively.	63
Figure 4.7	DOS (upper stack) and projected DOS (lower stack) of BP_V , and BP^N sheet before and after adsorption of (a,d) CO, (b,e) CO_2 , and (c,f) NH_3 molecules, respectively (red and black colour indicates DOS before and after adsorption; dark	64

yellow and purple colour indicates s orbital, pink and violet colour indicates p orbital of N and O atom, respectively).

Figure 4.8	Electron localisation function (ELF) plots of (a-c) CO, (d-f) CO ₂ , and (g-i) NH ₃ on BP _v ^N , BP _v , and BP ^N surfaces, respectively.	65
Figure 5.1	(a) top view, (b,c) side view of mixed phase SnS/h-BN heterostructure; (d,e) convergence test of lattice parameters vs. ground state energy.	75
Figure 5.2	Schematic representing the modelling process of the SnS/h-BN heterostructure.	75
Figure 5.3	AIMD simulation at (a) 300 K, (b) 450 K, (c) 600 K, and (d) 700 K (the axis on the left side of the figures represents the energy of the heterostructure and the axis on the right side of the figures represents the temperatures scale).	76
Figure 5.4	(a) Charge density difference plot of SnS/h-BN heterostructure (cyan and yellow colour represents the accumulation and depletion of charges, respectively); (b) electrostatic potential along the z-direction of SnS/h-BN heterostructure (inset: electrostatic potential of SnS monolayer); (c) electron localization function (elf) plot of SnS/h-BN heterostructure (the blue to red colour bar indicates the lowest (-1) to highest (1) value; (d) layer projected electronic band structure plotted along the X-Γ-Y-T-X high symmetric path (blue and red colour indicates the contribution from the SnS and h-BN monolayers, respectively); (e) orbital projected density of states (PDOS) of SnS/h-BN heterostructure; and (f) schematic showing the straddling type-I band alignment of SnS/h-BN heterostructure.	78

Figure 5.5	GW band structure of (a) SnS monolayer, (b) SnS/h-BN heterostructure (the dotted lines in the figures indicates to the bands calculated using DFT-GGA approach; the quasiparticle GW bands in (a) and (b) are represented by the violet, and the orange lines, respectively; the highest valence band (HVB) and the lowest conduction band (LCB) in (a), and (b) are represented by the red and wine coloured line, respectively); (c, d) illustrates the BZ and schematic representation of band gaps of SnS, and SnS/h-BN, respectively.	80
Figure 5.6	Optical absorption spectra of (a) SnS/h-BN heterostructure (the excitonic strength is indicated by the vertical drop line in a normalized scale of 0 to 1), and (b) SnS monolayer; average electron-hole density of (c) A_{SnS} , and (d) B_{SnS} exciton in the heterostructure (the magenta (top panel) and the cyan (bottom panel) colour represents the electron and hole density, respectively); schematic demonstrating the electron-hole pairs in (e) monolayer SnS without intralayer electric field, and (f) SnS/h-BN heterostructure with intralayer electric field (the solid black arrows on electrons and hole indicates the direction of force due to the electric field).	84
Figure 6.1	Relaxed atomic structures of the SnS/BNNT mixed-dimensional heterostructures for three different BNNT chiralities: (a) SnS/(5,0) BNNT, (b) SnS/(6,0) BNNT, and (c) SnS/(7,0) BNNT. Panel (d) illustrates the stacking orientation, where the BNNT axis is aligned along the armchair direction of the SnS monolayer.	96
Figure 6.2	(a-c) Convergence test for lattice parameters vs. ground state energy; (d) AIMD simulation of the SnS/BNNT heterostructures at 300 K.	97

- Figure 6.3 Charge density difference (CDD) plots of the mixed-dimensional heterostructures: (a) SnS/(5,0) BNNT, (b) SnS/(6,0) BNNT, and (c) SnS/(7,0) BNNT. Cyan and yellow regions indicate charge accumulation and depletion, respectively. The point x_0 along the x-axis marks the location of minimum interfacial separation. (d) Variation of interfacial separation, charge transfer, and BNNT diameter as a function of increasing chirality. Electron localization function (ELF) profiles for SnS/(n,0) BNNT heterostructures are shown in (e) $n = 5$, (f) $n = 6$, and (g) $n = 7$, confirming the van der Waals nature of interfacial interactions (the blue to yellow colour bar indicates the lowest (-1) to highest value (+1)). 98
- Figure 6.4 Planar-averaged electrostatic potential profiles of the mixed-dimensional heterostructures: (a) SnS/(5,0) BNNT, (b) SnS/(6,0) BNNT, and (c) SnS/(7,0) BNNT. The evolution of the intralayer potential difference (ΔV_{SnS}) and interfacial potential difference (ΔV_{hetero}) is illustrated, highlighting the transition from 2D/1D SnS/BNNT stacking to the 2D/2D SnS/h-BN configuration. 99
- Figure 6.5 Structure-projected electronic band structures of (a) SnS/(5,0) BNNT, (b) SnS/(6,0) BNNT, and (c) SnS/(7,0) BNNT heterostructures at the DFT-GGA level of theory. Blue and red colours represent the contributions from SnS and BNNT, respectively. The corresponding quasiparticle-corrected GW band structures are presented in (d-f), with solid lines indicating GW bands and dotted lines denoting DFT-GGA bands for comparison. To illustrate the evolution of the lower conduction bands under GW corrections, the two lowest conduction bands (C_1 and C_2) are highlighted in red and blue, respectively. 101

Figure 6.6	Optical absorption spectra of (a) SnS/(5,0) BNNT, (b) SnS/(6,0) BNNT, and (c) SnS/(7,0) BNNT heterostructures. Excitonic transition strengths are indicated by vertical drop lines, normalized on a scale from 0 to 1. (d) Spatial distribution of the averaged electron-hole density associated with the interdimensional exciton (IDE) in the SnS/(5,0) BNNT heterostructure; the pink and cyan regions represent the electron and hole densities, respectively. (e) Magnified view of the GW band structure of SnS/(5,0) BNNT near the Γ -point, illustrating the momentum-space distribution and transition weight of the IDE state.	104
Figure 6.7	Electronic band structures of the SnS/(5,0) BNNT heterostructure under uniaxial strain applied along the nanotube axis. Panels (a-c) show the band structures under compressive strain of -1%, -3%, and -5%, respectively, while panels (d-f) correspond to tensile strain of +1%, +3%, and +5%.	106
Figure 6.8	Optical absorption spectra of the SnS/(5,0) BNNT heterostructure under uniaxial tensile strain of (a) 1%, (b) 3%, and (c) 5%. The corresponding schematic illustrations in (d-f) depict the evolution of the C_1 and C_2 conduction bands with increasing tensile strain, highlighting the increase in the number of available IDE transition states across the Γ -X valley.	107
Figure A.1	Electrostatic potential of (a) BP_V^N , (b) BP_V , and (c) BP^N monolayer, respectively.	118
Figure A.2	Schematic illustration of (a) chemisorption and (b) physisorption on BP_V^N surface.	118

Figure A.4	Electronic band structure of BP_v^N , BP_v , and BP^N sheet after adsorption of (a-c) NO_2 , and (d-f) SO_2 molecules, respectively.	119
Figure A.5	Electronic band structure of (a-c) BP_v^N , (d-f) BP_v , and (g-i) BP^N monolayer after the adsorption of CO, CO_2 , and NH_3 molecule, respectively.	120
Figure A.6	(a) Electronic band structure and (b) optical absorption spectra of h -BN monolayer, respectively.	121
Figure A.7	Layer projected electronic band structure of SnS/ h -BN heterostructure with no strain on SnS layer, plotted along the X- Γ -Y-T-X high symmetric path (blue and red colour indicates the contribution from the SnS and h -BN monolayers, respectively).	121
Figure A.8	Band structure of (a) (5,0) (b) (6,0), and (c) (7,0) BNNTs; (d) optical absorption spectra of the BNNTs.	122

List of Abbreviations

0D	Zero-Dimensional
1D	One-Dimensional
2D	Two-Dimensional
ac	armchair
AIMD	Ab-Initio Molecular Dynamics
BNNT	Boron Nitride Nanotube
BP	Black Phosphorene
BSE	Bethe-Salpeter Equation
BZ	Brillouin Zone
CB	Conduction Band
CBM	Conduction Band Minimum
CDD	Charge Density Difference
CNT	Carbon Nanotube
DFT	Density Functional Theory
EBE	Exciton Binding Energy
GGA	Generalized-Gradient-Approximation
GW	Green's function 'G' with screened Coulomb potential 'W'
<i>h</i> -BN	Hexagonal Boron Nitride
HF	Hartree-Fock
HVB	Highest Valence Band
IDE	Interdimensional Exciton
IFE	Interfacial Exciton
KS	Kohn-Sham
LCB	Lowest Conduction Band
LDA	Local Density Approximation
MBPT	Many-Body Perturbation Theory
ONCPPSP	Optimized Norm-Conserving Vanderbilt Pseudopotential
PAW	Projector Augmented-Wave
PDOS	Projected Density of States
PPA	Plasmon-Pole Approximation
PV	Photovoltaics
QP	Quasiparticle

RPA	Random Phase Approximation
SCF	Self-Consistent Field
SnS	Tin(II) Sulfide
TMDC	Transition Metal Dichalcogenide
TMMC	Transition Metal Monochalcogenide
VB	Valence Band
VBM	Valence Band Maximum
vdW	Van der Waals
zz	zigzag

List of Symbols

h	Planck's constant
U_{ei}	electron-ion interaction
W^H	Hartree potential
T	kinetic energy operator
H	Hamiltonian
e	electron
N	number of electrons
U_{ee}	electron-electron interaction
$T_{TF}[n]$	Thomas-Fermi kinetic energy functional
$n(r)$	electron density
ψ	wavefunction
E_{el}	electronic energy
$F[n]$	universal functional
V_{ext}	external potential
$E_{xc}[n]$	exchange-correlation energy
$v_{KS}(r)$	Kohn-Sham potential
$V_{xc}(r)$	exchange-correlation potential
$V_{pseudo}(r)$	potential mimicking the bare nuclear Coulomb potential and the effects of the core electrons
k	point in Brillouin Zone
$G_{nk}^0(\omega)$	non-interacting Green's function
f_{nk}	occupation factor
$G_{nk}(\omega)$	exact Green's function
$\Sigma_{nk}(\omega)$	GW self-energy
χ	response function
$\Omega_{GG'}$	plasmon frequencies
E_{nk}^{QP}	quasiparticle energy
Z_{nk}	renormalization factor
E_{ck}	quasiparticle energies of conduction band
E_{vk}	quasiparticle energies of valence band
A_{vck}^S	exciton amplitude

Ω^s	exciton eigenvalue
K^{eh}	electron-hole interaction kernal